Analysis of frequency content of temperature glider data via Fourier and wavelet transforms

I. Mancero-Mosquera[1], P.M. Poulain[1], R. Gerin[1], E. Mauri[1], D. Hayes[2], P. Testor[3] and L. Mortier[3]

[1] *Istituto Nazionale di Oceanografia e di Geofisica Sperimentale, Trieste, Italy*
[2] *Oceanography Centre University of Cyprus, Nicosia, Cyprus*
[3] *Université Pierre-et-Marie Curie, Paris, France*

ABSTRACT   A methodology to analyze the spectral content of glider data is proposed by showing the application to time series taken during missions in the Mediterranean Sea. Three missions have been investigated, two in the Tyrrhenian Sea and one south of Cyprus. Fluctuations appearing in temperature series recorded by gliders are studied with the help of the Fourier and wavelet transforms. The Fourier transform has been used to localize high energy in a certain range of frequencies, which is limited by the experimental setting or sampling rate. The obtained information together with additional analysis via the wavelet transform provide a way to localize these features in time and in space, allowing a better understanding of their nature and physical meaning.

1. Introduction

Gliders are unmanned autonomous vehicles that allow the measuring of oceanographic properties by performing a series of angled profiles, up and down, along a pre-planned path. Their low power consumption makes them suitable for long missions, needing only remote monitoring for carrying out the mission, and human assistance at the deployment and recovery (Ericksen *et al.*, 2001; Rudnik *et al.*, 2004). Profiles reach a maximum depth that depends on instrumental limitation and the sea bottom. The recurrent movement up and down through the water column, as well as the path being followed by the glider, typically introduces cyclic behaviour in the observational data streams. This, together with normal limitations of sensors such as time lags, and the framework characterized by the displacement of the vehicle and the medium (Bishop, 2008; Garau *et al.*, 2011), present challenges to be tackled when searching for frequency content in the data. In the present work, analysis schemes based on Fourier and wavelet transforms are applied to temperature records from gliders in several missions in the Mediterranean Sea under different conditions.

2. Missions and experimental set-up

Three missions have been selected for the analysis, namely the LIDEX-10 (L10) and Tyrrmount-09 (T09), both located in the Tyrrhenian Sea, and the Eye of Levantine (EoL) mission south of Cyprus. Spatial references to the missions are shown in Fig. 1.
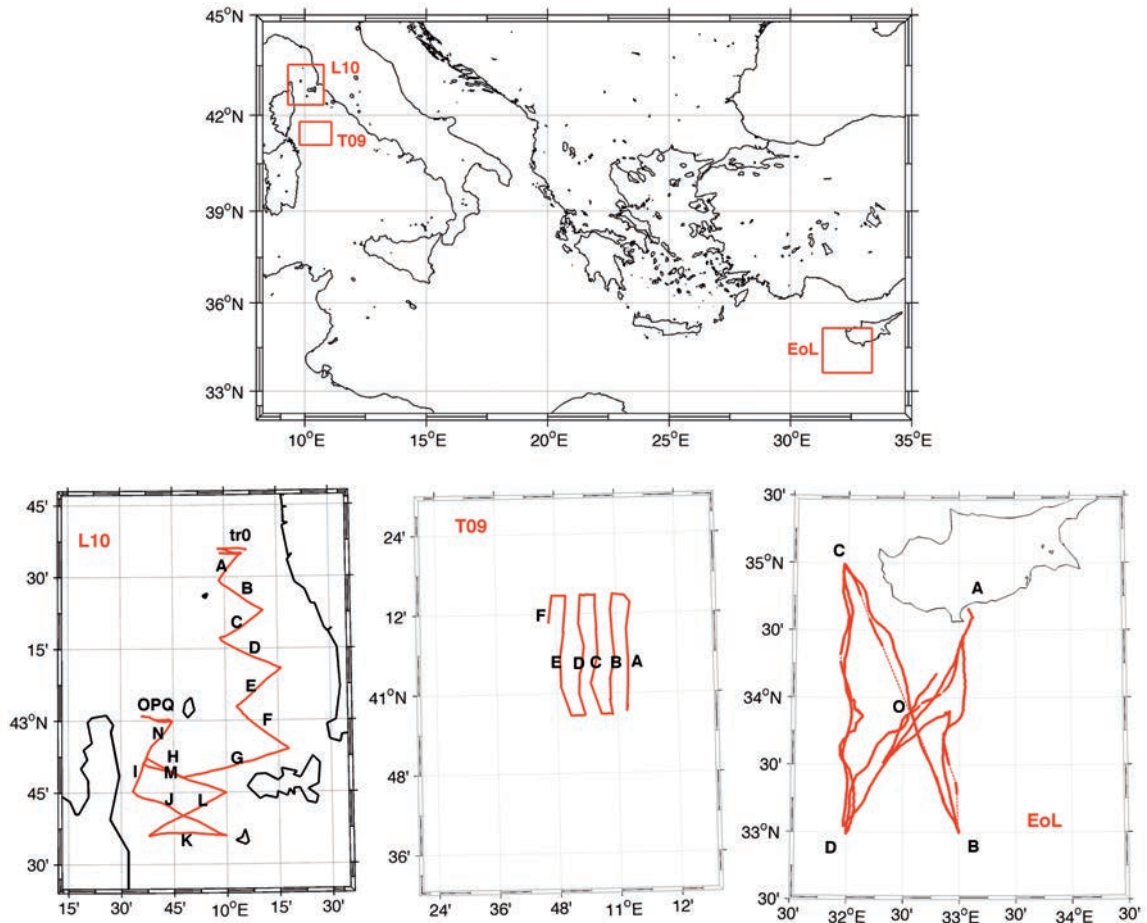
Fig. 1 - Areas of study and glider trajectories corresponding to missions L10, T09, and EoL.

The sampling scheme usually consists of a series of up and down profile casts, along a path defining a sequence of transects performed around some features of interest. In L10, a number of transects were made along the expected trail of the Arno river plume along the Italian coast, before proceeding to deeper areas in the Corsica channel (Mauri *et al.*, 2013). The mission was carried out between July 2 and 20, 2010, corresponding to a strong stratification of the sea resulting from summer solar insolation. The EoL mission was intended to monitor the anti-cyclonic Cyprus Eddy (Hayes *et al.*, 2011), thus a "butterfly" sampling pattern was designed to perform several transects across the structure between November 2009 and March 2010. Likewise, the T09 mission was a sequence of transects oriented along the N-S direction in order to study the dynamics of the area over the Vercelli seamount, from May 23 to 30, 2009 (Mauri *et al.*, 2010). Table 1 summarizes the sequences of transects comprising the total trajectories of the missions, with their corresponding length and duration.

The velocity during the descending path of the glider is usually slightly different than the one during the ascending period, with different permissible angles of inclination in each case. This asymmetry in the pair of profiles can introduce fake oscillations in the records of the measured

Table 1 - Length and duration of transects in the three studied missions: L10, T09 and EoL.

L10			span		T09			span	
label	Start time	UTC	*day*	*km.*	label	Start time	UTC	*day*	*km.*
Tr0	2 Jul 2010	12h06	3.2	45.8	A	23 May 2009	10h53	1.1	34.4
A	5 Jul 2010	16h08	0.5	14.1	B	24 May 2009	17h05	1.3	35.4
B	6 Jul 2010	03h48	0.7	20.0	C	26 May 2009	04h19	1.2	35.1
C	6 Jul 2010	20h30	0.9	22.4	D	27 May 2009	13h08	1.3	34.3
D	7 Jul 2010	18h52	1.0	27.1	E	28 May 2009	23h04	1.2	34.5
E	8 Jul 2010	18h20	0.8	22.8	F	30 May 2009	07h29	0.3	7.6
F	9 Jul 2010	12h25	0.9	27.1	EoL			span	
G	10 Jul 2010	10h49	1.6	43.2	label	Start time	UTC	*day*	*km.*
H	12 Jul 2010	01h25	0.5	16.4	AD	23 Nov 2009	10h28	9.0	151.7
I	12 Jul 2010	12h28	0.5	15.4	DO	2 Dec 2009	09h28	4.3	91.6
J	13 Jul 2010	01h14	1.4	41.0	OB	6 Dec 2009	17h34	5.6	107.3
K	14 Jul 2010	10h24	1.4	31.6	BC	12 Dec 2009	08h04	10.7	252.5
L	15 Jul 2010	19h29	1.4	36.3	CD	23 Dec 2009	00h30	11.9	237.0
M	17 Jul 2010	03h50	1.2	34.1	DA	3 Jan 2010	23h05	9.0	194.8
N	18 Jul 2010	08h27	0.9	22.6	AB	12 Jan 2010	22h51	7.2	154.2
OPQ	19 Jul 2010	07h15	1.0	24.3	BC	20 Jan 2010	04h23	15.2	271.8
					CD	4 Feb 2010	08h21	15.2	289.1
					DA	19 Feb 2010	13h23	11.7	200.2

parameters. Local bathymetry also influences the time interval of the down-cast/up-cast profiles, implying the instrument does not always travel the same horizontal distances between surfacings.

The Slocum glider TENUSE used in the L10 mission had a mean forward speed of 40 cm/s, with average pitch angles of -26° and +28° for the down-cast and up-cast profiles, respectively. This means the horizontal speed is roughly about 35 cm/s, while the vertical component of velocity is between 17 and 18 cm/s. These are rough estimations, i.e., not taking into consideration local dynamics, changes in the water buoyancy, currents, etc. The L10 mission area contains varying bathymetry, and thus a pair of profiles can be completed in about six minutes for a 70 m depth, while it can take about 34 minutes for the full 200 m depth range of the utilized glider. Likewise, the horizontal separation at the surface is about 270 m for data in a pair of profiles in a 70 m depth area, while the separation at the surface can reach 780 m for the maximum depth of 200 m. The instrumental sampling rate depends on the glider's on-board data logger. The glider used for the L10 mission provided data with four- or eight-second time resolution. In the most common case, the vertical separation between measurements was about 1.4 - 1.5 m, corresponding to a horizontal distance between the measurements of about 3.2 m, according to the pitch.

In the T09 mission, the Slocum glider Trieste-1 provided measurements every four seconds. The monitored area is deep and the glider consistently reached a maximum depth of about 180 m, which implies a horizontal separation of about 780 m at the surface for a pair of consecutive profiles, with a time interval of roughly 36 minutes.

In contrast, the Seaglider ATALANTA from the EoL mission reached 1000 m of depth, completing a pair of consecutive down-cast/up-cast profiles in about seven hours, and thus the separation of profiles at the surface is about 4 - 6 km, depending on local conditions such as currents. The sampling interval for temperature data provided by the EoL mission glider is five seconds.

These data provide an example of the spatial resolution that can be obtained from the glider platform. The way a mission is designed is important, since it can introduce oscillations in the records according to the path followed by the glider. The timescale of the displacements has to be kept in mind before any interpretation is made. Physical separation is at the maximum at the surface for consecutive down-cast/up-cast profiles, and thus that is the coarsest spatial resolution. Likewise, the typical time for completion of a given pair of profiles is the coarsest time resolution, which will be important in the following analysis.

3. Measurements

Temperature has been selected for analysis due to its relatively short sensor time response. Other parameters, such as conductivity or dissolved oxygen concentration, have relatively long response times (Bishop, 2008), which would impede the kind of analysis proposed here. It would make sense to analyse the density record, from a physical standpoint. However, the density is computed from salinity, temperature, and pressure, while salinity is computed from conductivity and temperature. Any time lag and consequent error in conductivity and temperature records would propagate through the formulation until the yielded density. Any oscillation found in the temperature record is an indication of changes in the properties of the water mass as detected by the glider. These changes may be due to the glider moving horizontally or vertically through different water masses, as well as vertical movement of the water such as vertical mixing or internal waves occurring along the thermocline. Fig. 2 shows the entire records of temperature corresponding to the described missions.

4. Methods

4.1. Preliminary treatment of temperature data

Temperature data were organized in a regular grid having 1 m vertical resolution and 5-minute horizontal resolution.

The depth recorded in the data set is uneven due to a possible irregular sampling rate (as in the L10 mission) and to a variable speed of the glider along the water column, which occurred during the thermocline crossing or while navigating through different densities.

Temperature series were generated by simple linear interpolation with 1-m step vertical resolution. Corresponding times are then obtained via the same interpolation.

The asymmetry in the cycle of down-cast/up-cast profiles due to different pitch angle during descending and ascending phases introduces additional nuisances in the form of spurious oscillations. Therefore, a better result quality is assured by taking only up-cast profiles, even though this corresponds to a loss of data and to a reduction of horizontal resolution.
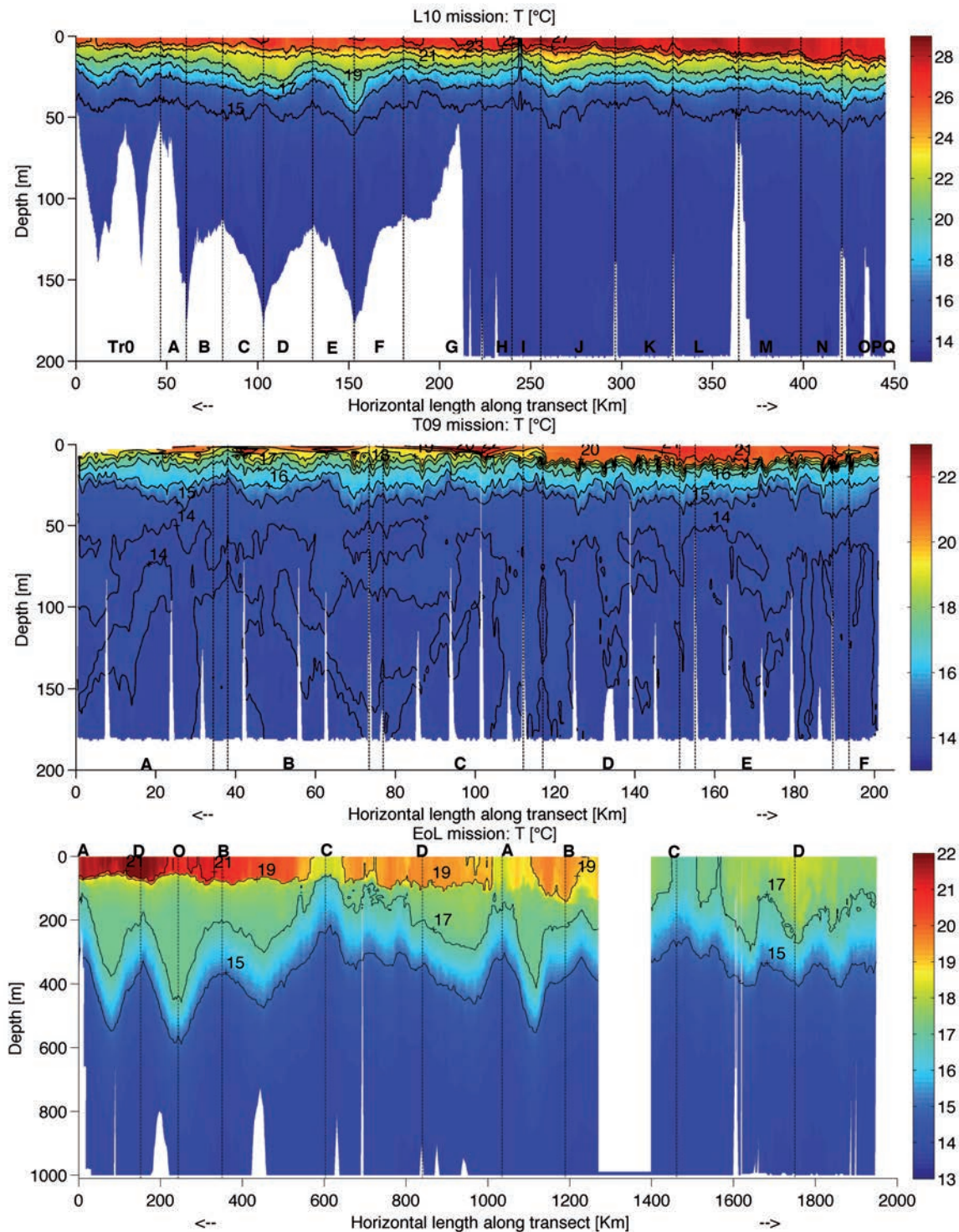
Fig. 2 - Temperature fields from L10 (upper panel), T09 (mid panel) and EoL.

The second stage is to interpolate horizontally in order to obtain a regularly sampled time series for every fixed depth. A 5-minute sampling rate is chosen (i.e., 12 samples per hour), so that the produced series will lose minimal information in the shallower profiles, while becoming redundant in the deeper ones. The Nyquist frequency for the Fourier spectra under these conditions will be six cycles per hour (cph). Interpolating schemes do not add information to the data, but make the same information available on a regular grid (Jenkins and Watts, 1968).

The Fourier transform and the overlapping Hamming data window were applied to the regular series at each depth level, and the power spectra were derived. The panels of Fig. 3 show this bulk application for the three missions. In the top panel of Fig. 2, the full L10 temperature record shows that only the top 50 m are always sampled, so the spectra for the L10 mission were computed down to a depth of 50 m. On the other hand, T09 and EoL contain continuous records down to 180 and 1000 m depth respectively, and thus the spectra were computed accordingly.

4.2. The Fourier transform

The Fourier transform is well documented in the literature, being in wide use for the analysis of frequency in time series. However, a brief description is provided for the sake of completeness and to allow a better comparison with the wavelet transform. The Fourier transform of a function $f(t)$ is computed via an integral of the form:

$$\left|\hat{f}(\omega) = \langle f, \exp(j\omega t)\rangle = \int_{-\infty}^{+\infty} f(t) \exp(-j\omega t)dt\right|, \tag{1}$$

where t denotes time, ω the frequency and $\langle,\rangle$ indicates the inner product in the Hilbert space of functions with finite energy. The inner product implies a scalar projection of $f(t)$ over the orthogonal set of functions $\exp(j\omega t)$, and thus the energy of f is captured by the transformation coefficients in a conservative way, i.e., the energy of f and $\hat{f}$ are equivalent.

Detailed algorithms to estimate the Fourier spectra are found in the literature (Press *et al.*, 1992). Best practices include the separation of the record in data windows, such that the corresponding Fourier spectra are averaged later (Jenkins and Watts, 1968). There are also several ways to normalize the transform to account for conservation of the energy, or the variance (equivalent to average energy), as well as to take into consideration real or complex time series. Here, variance-conservation normalization is chosen, so that the integral of the spectra corresponds to the total variance (equivalent to power or average energy) of the time series. Hereafter, every Fourier spectra shown is a "power spectrum", with the general expression:

$$Psd_T = \frac{1}{k} \sum_{over\ i} \left|\frac{Psd_i}{U_w W_L}\right|,$$

where Psd_T is the total power spectrum, computed as the sum of the partial spectra from every data window, Psd_i. Here, Psd_i is the square modulus of the Fourier transform of the ith data window. U_w is the energy introduced by the window, here chosen to be of the Hamming type. Finally, the number of windows k depends on the length of the window (W_L), the length of the record being split, as well as the overlapping chosen between consecutive data windows (50% unless otherwise specified). Thus the Fourier spectra exist between 0 and the Nyquist upper limit with a frequency resolution of $1/W_L$.
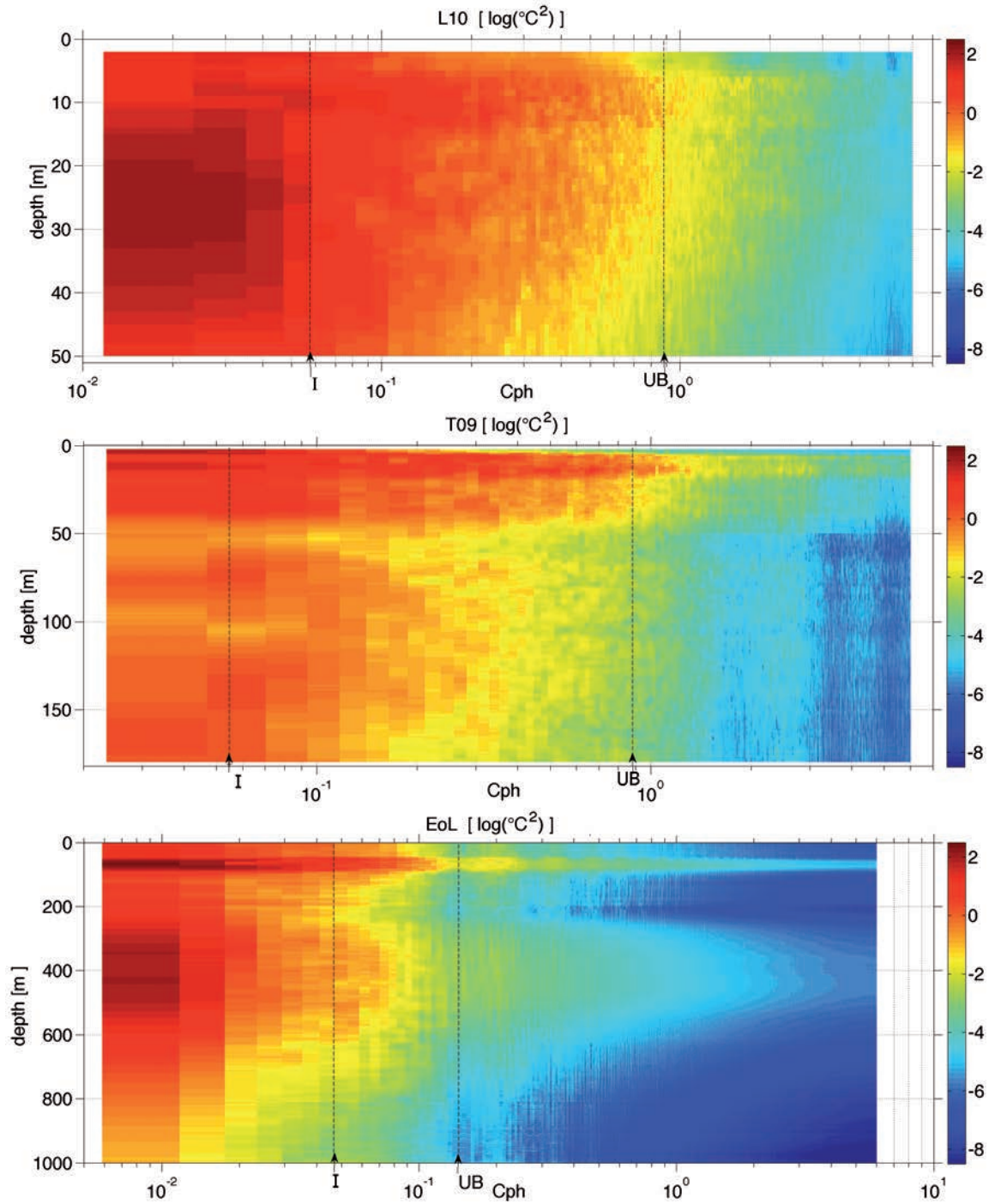
Fig. 3 - Fourier spectra on a level-by-level basis with 1-m vertical resolution for the three missions.

4.3. The wavelet transform

The wavelet transform is performed via an integral of the form:

$$\tilde{f}(s,\tau) = \langle f, \psi_{s,\tau} \rangle = \int_{-\infty}^{+\infty} f(t)\, \psi_{s,\tau}^{*}\, dt \ , \tag{2}$$

where * indicates complex conjugation. The function $\psi_{s,\tau}$ is a translated and scaled version of the so-called "mother wavelet" function, ψ:

$$\psi_{s,\tau} = \frac{1}{\sqrt{s}} \psi\left(\frac{t-\tau}{s}\right).$$

The wavelet transform and the linear filtering process are related, because the translation parameter (τ) makes Eq. 2 a convolution, where ψ is acting as a filter. The s parameter changes the scale of ψ, thus changing its frequency of oscillation. The function ψ is defined as a transient wave with zero mean that decays to zero outside of a short interval, as opposed to the perennial-oscillating sinusoids of the Fourier theory (Mallat, 1999). In the discrete formulation, τ varies according to the sampling rate, $\tau = n\Delta t$, $n \in \mathbb{Z}$; while s is dyadic (i.e., a power of two), $s = 2^j$, $j \in \mathbb{N}$. Thus, j changes the scale of ψ so that the integral corresponds to a band pass filtering process, capturing portions of the spectrum at different frequency intervals. The interval limits are indicated as periodicity in time units, according to the expression ($2^j\Delta t$, $2^{j+1}\Delta t$) and properly renamed "timescales". There are several algorithms devised to compute the wavelet transform such as the continuous transform, the time-invariant transform and the orthogonal transform. It is often possible to do the calculations via an associated filter instead of the original wavelet function, mainly when there is no explicit mathematical expression available for the wavelet function (Daubechies, 1992).

For the present work, the time-invariant transform is selected since it performs a filtering of data so that features are traceable to the original time series. Similar filtering is done under the orthogonal transform, but shrinking the number of filtered coefficients makes it difficult to relate the features to the original data.

Likewise, the least-asymmetry wavelet function, also known as Symmlet, is chosen for its suitable properties. Symmlet functions have compact support; its associated filter has a finite number of coefficients and a near-linear phase response. The latter property allows for a good alignment of the filtered series with the original data vector, so that any variation of energy in the data can be located in specific time and space intervals.

5. Results and discussion

5.1. Application of the Fourier transform

In the case of the L10 mission, two consecutives profiles of the same direction have a time separation at the surface of about 34 minutes, which implies a maximum frequency of 0.88 cph with actual physical significance. This upper boundary is labelled "UB" and indicated with vertical dashed lines in the spectra. UB is computed like the Nyquist frequency, albeit using the average separation between actual measurements instead of the one between interpolated data. Another frequency of interest is the one corresponding to inertial oscillations (labeled "I" in
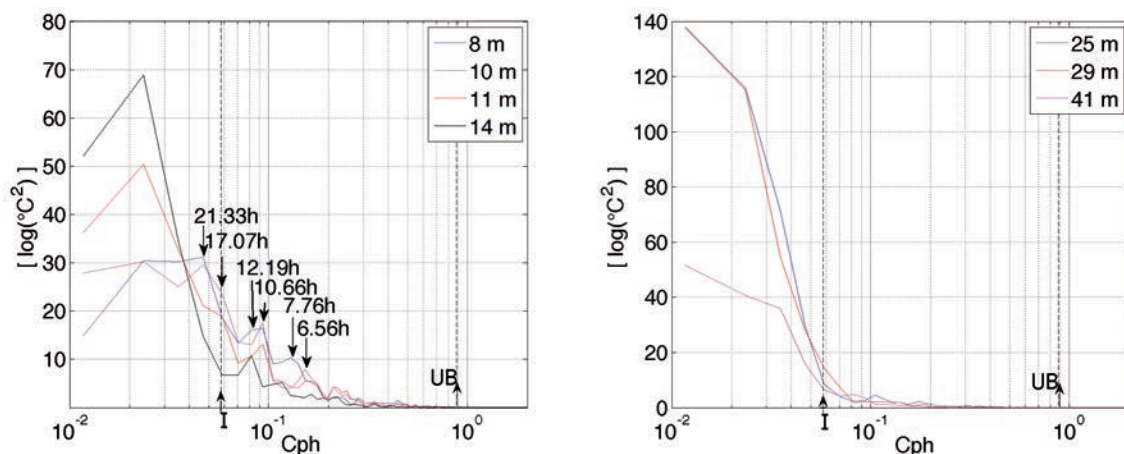
Fig. 4 - Spectra at selected depths (from the Fourier spectra) of L10, in the thermocline (left panel) and outside the thermocline (right panel).

figures). In L10, inertial oscillations are expected to have a period of about 17.6 h, as indicated in Fig. 3 (upper panel).

It can be seen that there are some layers where the spectra are more energetic. One of them is a horizontal band between 5 and 15 m of depth in correspondence with the thermocline. A second one is between 20 and 30 m in the lower frequencies. Several horizontal slices at selected depths are shown in Fig. 4; spectra at the thermocline level are shown in the left panel, while the right panel contains spectra in the second layer of interest.

Simulated seas with horizontally uniform temperature fields (not shown here), containing no oscillation, offer a way to assess the significance of the spectra peaks from the real mission by comparing it against this background of noise. In order to assess the possible effects of the experimental setting on the Fourier spectra, a simulation was performed by constructing a constant and uniform temperature profile, and sampling it with the same rates and velocity as the glider in the real mission. The temperature is the average profile of the whole mission.
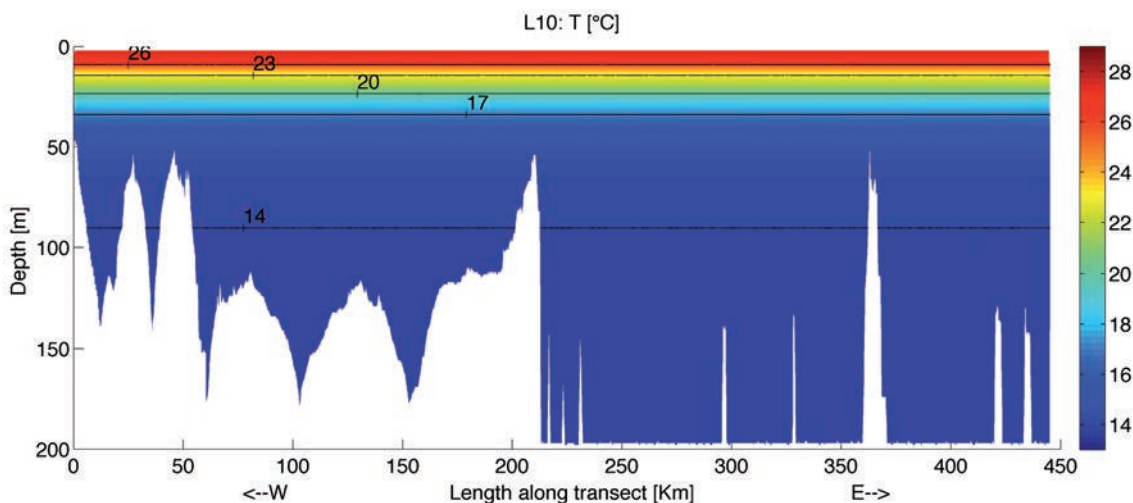

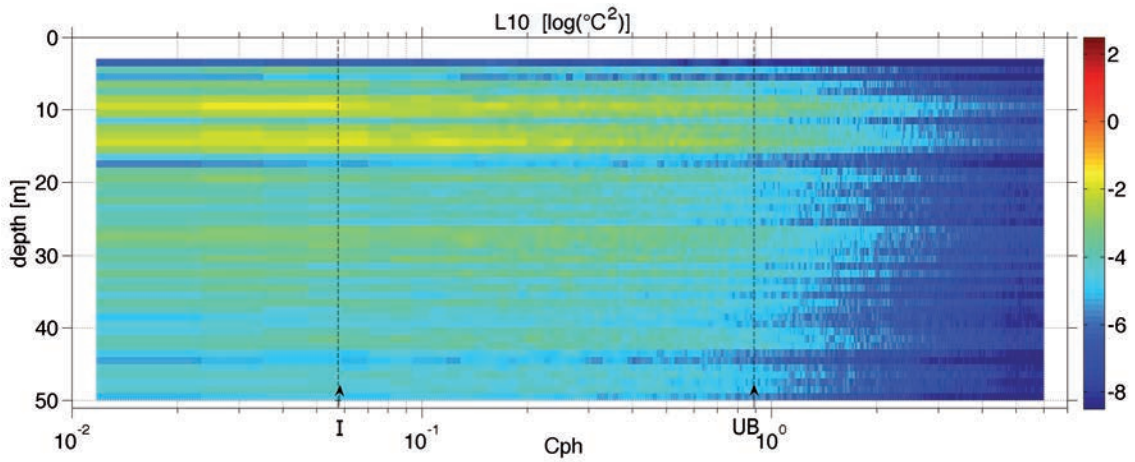Fig. 5 - Synthetic sea with a constant temperature gradient during the L10 mission.

Fig. 6 - Spectra of the simulated data of L10, as would be measured by the glider, and interpolated to a regular grid. The low energy is a by-product of the sampling scheme.

The glider is made to sample this temperature field at the original L10 rates. Then the data are processed as before, obtaining a matrix of 1-m depth and 5-minute time interval resolution. The generated map for the mission L10 is shown in Fig. 5, while the spectra are presented in Fig. 6. The results show that spurious oscillations are being produced as a result of the combination of sampling and interpolation schemes, since the simulated sea lacks horizontal oscillations. However, the energy of the spurious oscillations is several orders of magnitude less than the ones found in real conditions, as seen in the comparison in Fig. 7 and in the colour scales.

The procedure of extracting spectra at specific depths and comparing them with the spurious oscillations obtained from the synthetic sea was repeated for the T09 and EoL missions. Several spectra at selected depths from the T09 mission are presented in Fig. 8, and the vertical slices and background noise are shown in Fig. 9. Inertial oscillations are expected to have a periodicity of about 18.3 h in the T09 area. Similar results are presented in Figs. 10 and 11 for the EoL
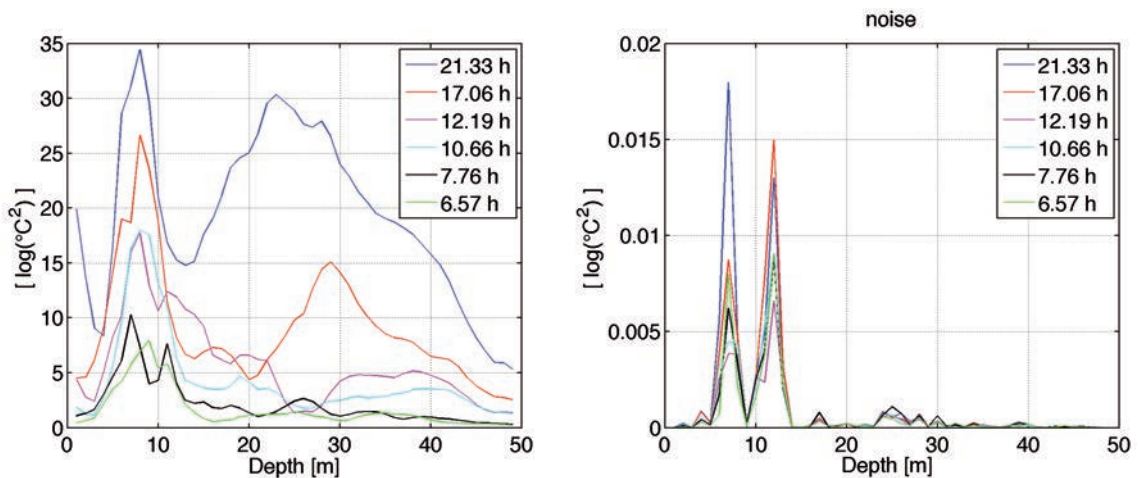

Fig. 7 - Left: vertical slices of L10 spectra with the frequencies indicated in Fig. 4. Right: the noise power spectra show local maxima at about 9 m, 11 m and 25 m of depth.
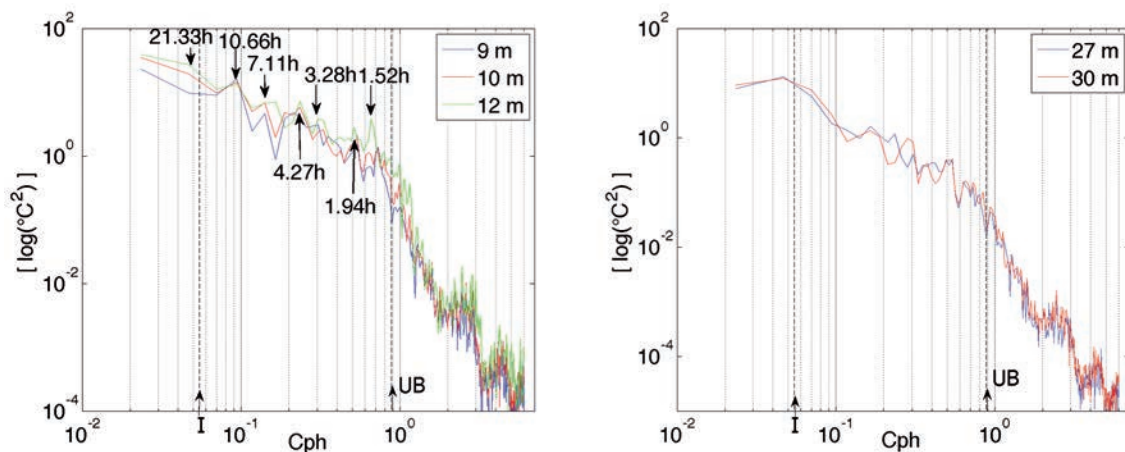
Fig. 8 - Horizontal slices from the T09 spectra for several depths in the thermocline (left panel) and outside the thermocline (right panel).

mission, where inertial oscillations have a period of about 21.5 h. Due to the larger scales of the mission EoL, the upper boundary of physical significance is 1/7 or 0.143 cph in the spectra.

5.2. Application of the wavelet transform

The Fourier transform allows the **identification of significant frequencies contained in** the data set. However, the complementary information on the localization of such signals is provided by the wavelet transform. The discrete formulation of wavelet transform yields coefficients ordered by intervals of periodicity or "timescales". Wavelet timescales are dyadic, i.e., increase in size by a power of two. Since the sampling rate has been interpolated, $\Delta t = 5$ min., the first timescale resolved by the transform is in the interval (10 min., 20 min.). The second timescale will be in the interval (20 min., 40 min.), generally fitting to the form: $(2^j \Delta t,$ $2^{j+1}\Delta t)$, $j = 1, 2, \ldots n$, $n \in \mathbb{N}$. The parameter j takes the name of "level of decomposition". An
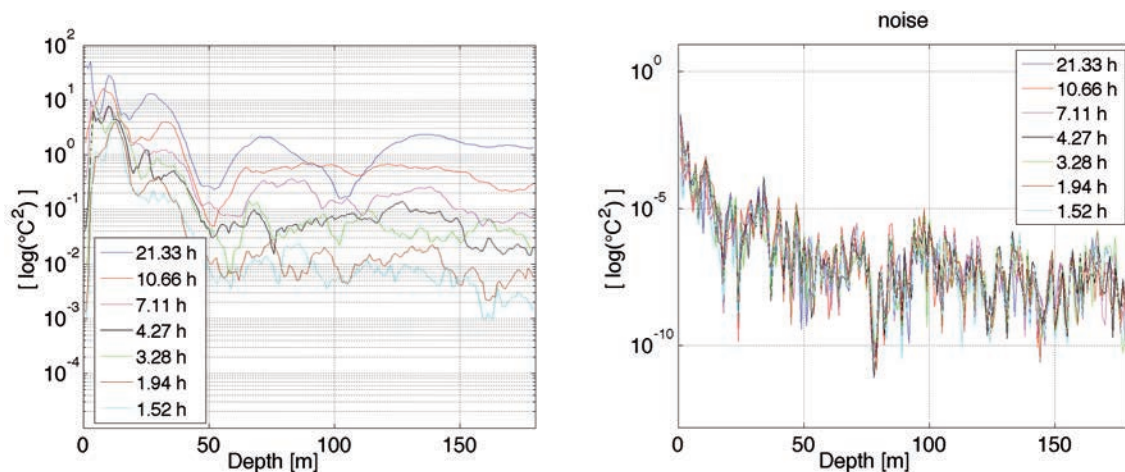

Fig. 9 - Vertical distribution of power for the frequencies indicated in Fig. 9 and corresponding noise power (T09 mission).
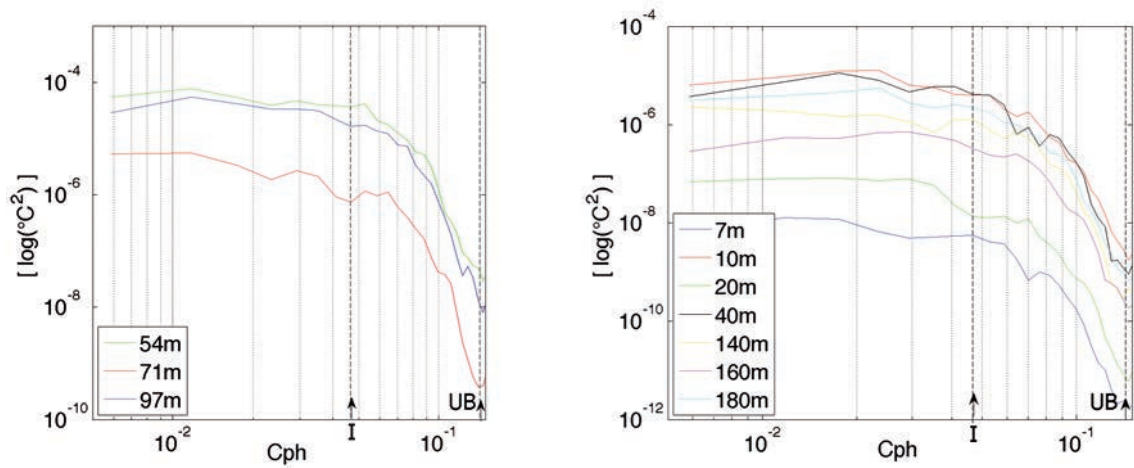
Fig. 10 - Horizontal slices from the EoL spectra, for several depths in the thermocline between 50 and 100 m (left panel), and outside the thermocline (right panel).

extensive plot of all the levels will not be presented in this work; only specific levels with significant information will be considered.

5.2.1. Tenuse-Lidex 10 (L10)

Complete wavelet energy spectra were generated for every level, from which two timescales ($j = 4$ and $j = 7$) are presented in Fig. 12. The first one, containing relatively short periodicities of between 1.33 and 2.66 h, shows a well-localized irregularity in the temperature series on July 12, in the transect "I". Under the Fourier theory, this kind of phenomenon introduces energy at high frequencies, making the spectra decay relatively slow (Mallat, 1999). The maximum energy is detected at 8 m of depth. The Fourier spectrum at the same level (see Fig. 4) is slower to decay. Most of the frequencies show a local maximum in a region of about 8 m of depth (as in
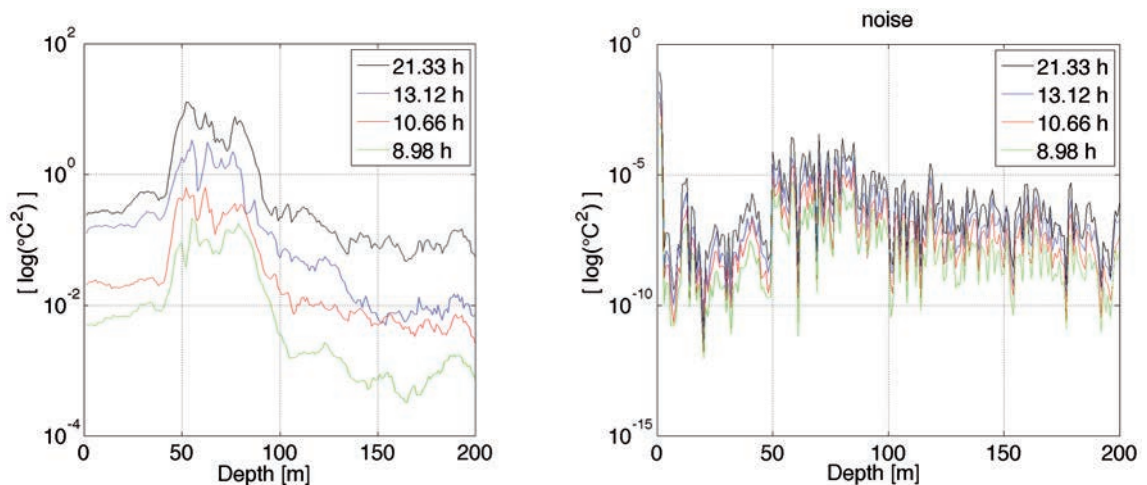

Fig. 11 - Vertical distribution of power for several frequencies and corresponding noise from the EoL mission.
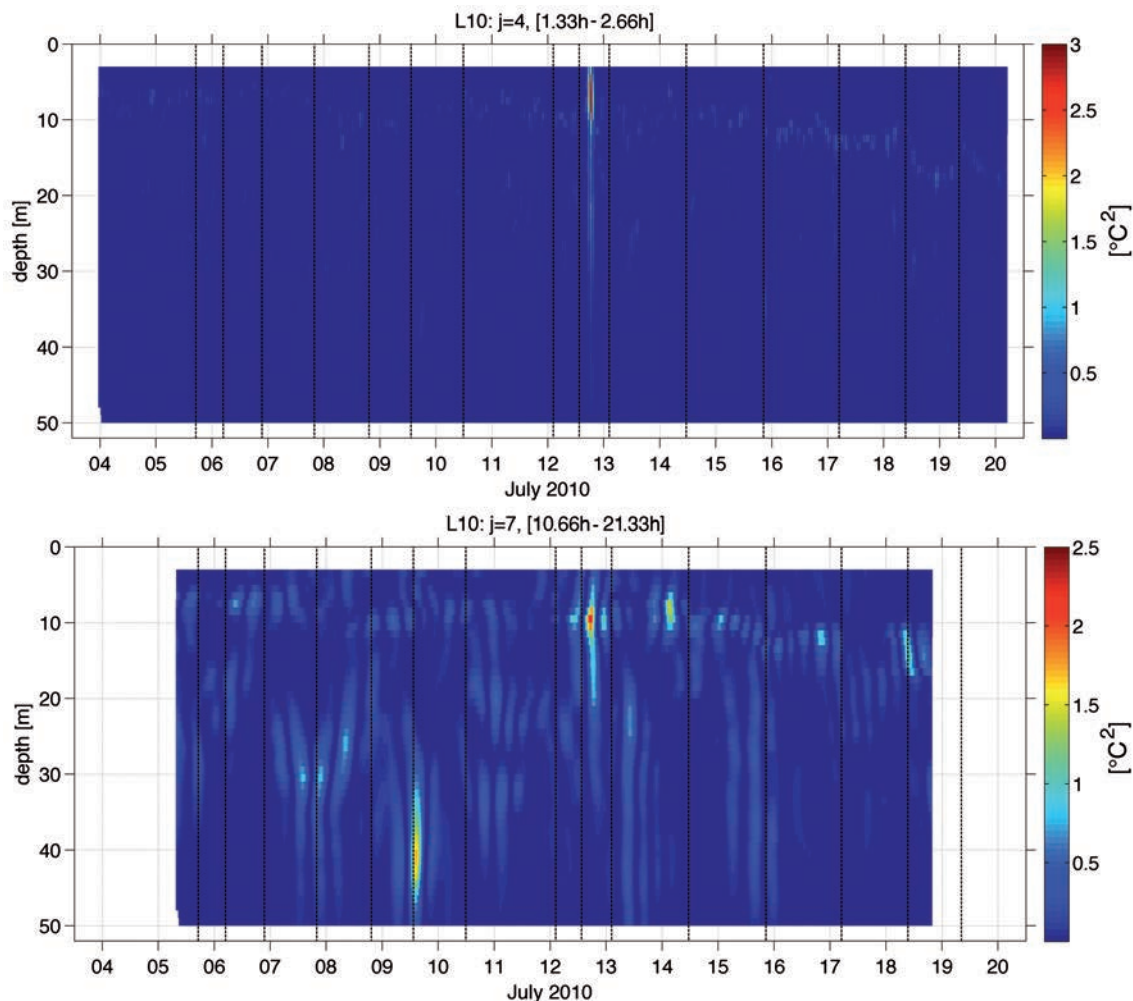
Fig. 12 - Selected timescales from the L10 wavelet analysis. The upper panel shows a transient feature appearing between July 12 and 13. Longer-scale features are shown in the lower panel.

Fig. 7). However, the wavelet spectra show that a well-localized irregularity is the reason for the behaviour of Fourier coefficients at that depth. The reconstruction of the temperature series at the time of the irregularity shows a collapse of the series to a lower value (Fig. 13, left panel), at first glance consistent with a cyclonic curl favouring upward flow of colder water from deeper layers. However, further analysis indicated that the transient feature was due to an instrumental failure in the recording clock.

The second wavelet spectra contain oscillations with periodicities between 10.66 and 21.33 h, appearing for the most part in the area of the thermocline. This timescale thus includes the inertial oscillation, with a period of about 17 h. A strong local maximum appears between 35 and 45 m of depth on July 9, however, near the limit between transects "E" and "F". A closer look reveals that the glider sampled a warmer and saltier water mass intruding from the west (Fig. 13, central and right panels).
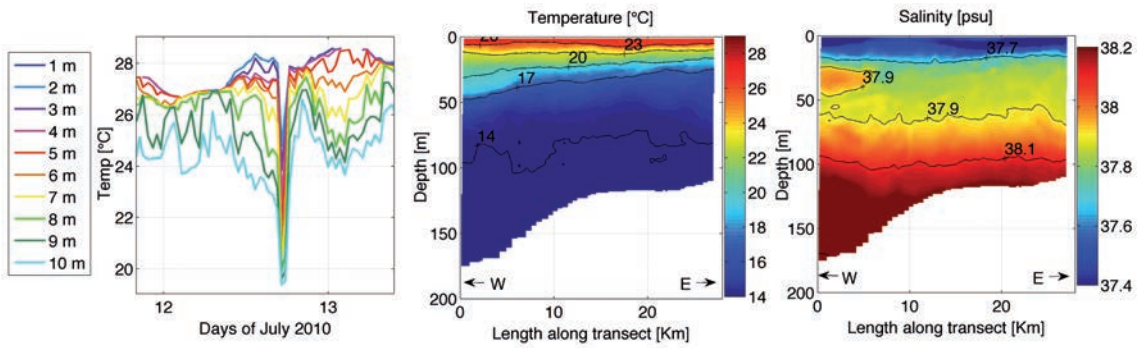
Fig. 13 - Left: reconstruction of temperature series at the time of the detected irregularity. Centre and right: intrusion of warmer and saltier water mass detected at the 10.66 and 21.33 h timescale.
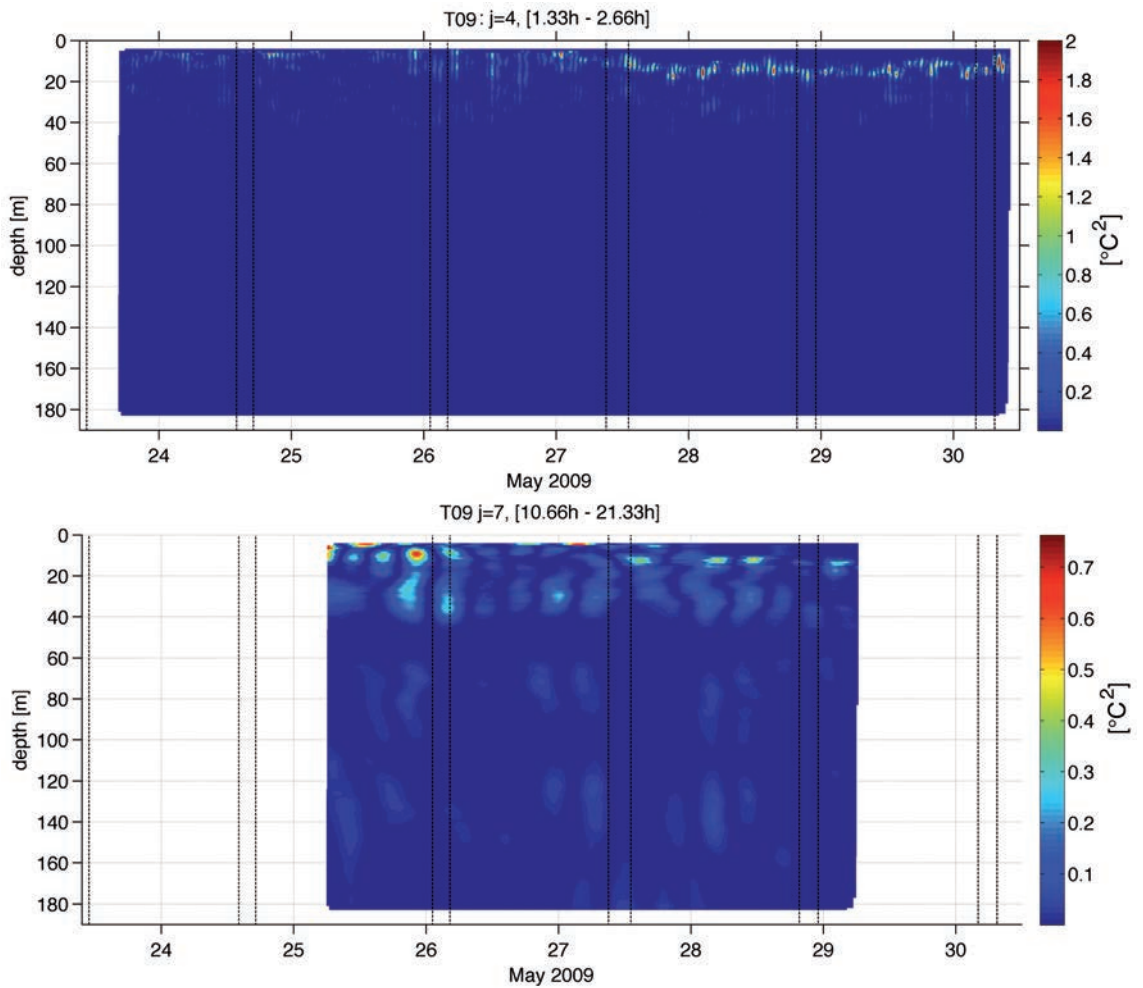

Fig. 14 - Selected timescales from the T09 wavelet analysis. Higher variability in the thermocline is visible in both panels. Lower panel: local maxima appear between 20 and 30 m of depth at timescales of between 10.66 and 21.33 h
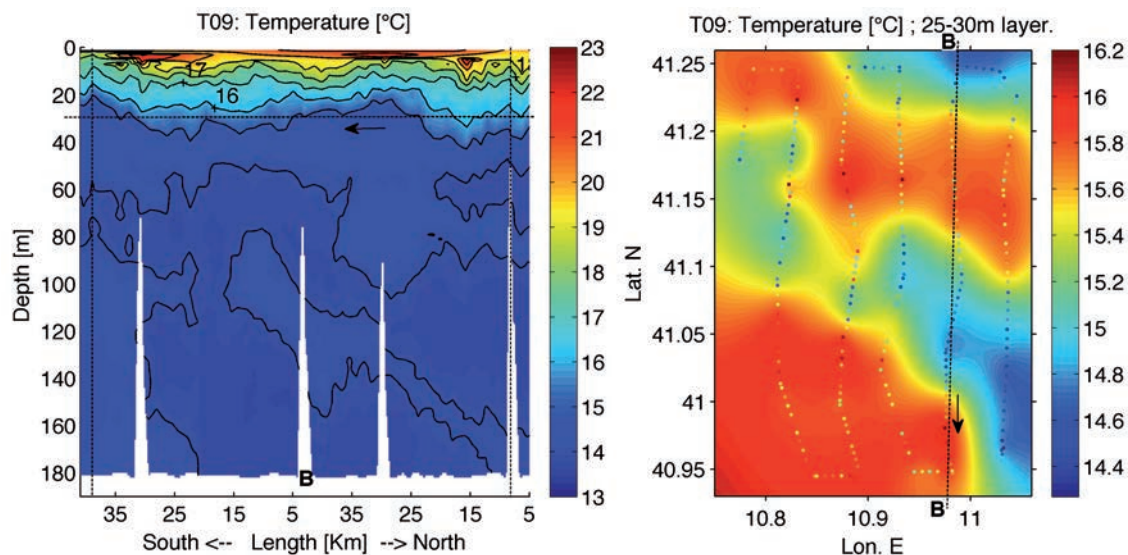
Fig. 15 - Temperature fields from the T09 mission. Transect "B" (left panel) and the horizontal layer between 25 and 30 m depth show the features at timescales of between 10.66 and 21.33 h.

5.2.2. Tyrrmount mission (T09)

Similar wavelet maps were selected for the T09 mission, i.e., containing the same periodicities as in the case of L10, and are shown in Fig. 14. This mission is considerably shorter so that loss of data in the boundaries, one of the shortfalls of the wavelet transform, is visible in the panels. Loss of data in the border of series increases as the timescale (*j* parameter) grows. There exists a different kind of irregularity in the data, in the form of a sudden deepening of the thermocline at the beginning of transect "D", when a warmer water mass in the surface pushed down the isothermals. This kind of feature (a "jump") is known to produce an increase of the power of high frequencies, making the energy slowly decay, as seen in the spectra in Figs. 2 and 9, at the thermocline level. The deepening of the thermocline can be observed in both wavelet spectra in Fig. 14.

At the timescale of between 10.66 and 21.33 h periodicities, features appear between 20 and 40 m depth, becoming stronger at the end of the transect "B", as can be seen in Fig. 15 with more detail. The reconstruction of the field temperature indicates that the features appearing in the wavelet spectra are due to the sampling by the glider of the shown spatial structures.

5.2.3. Eye of the Levantine (EoL) mission

The duration and spatial extent of the EoL mission provide longer time series for all depths, but also a coarse spatial resolution since the time for completing a monitoring cycle (down-cast/up-cast) increases up to about seven hours, given the 1000-m maximum depth reached by the instrument. The relevant wavelet levels are shown in Fig. 16. Features at the relatively shorter timescales (*j* = 7) appear in the area corresponding to the thermocline, disappearing towards the end of the record. Features in the deeper regions are significant at longer timescales; the structure being monitored (Cyprus Eddy) still does not yield a trace at *j* = 9, i.e., timescales between 1.75 and 3.54 days. However, there is a slightly stronger variability between 400 and
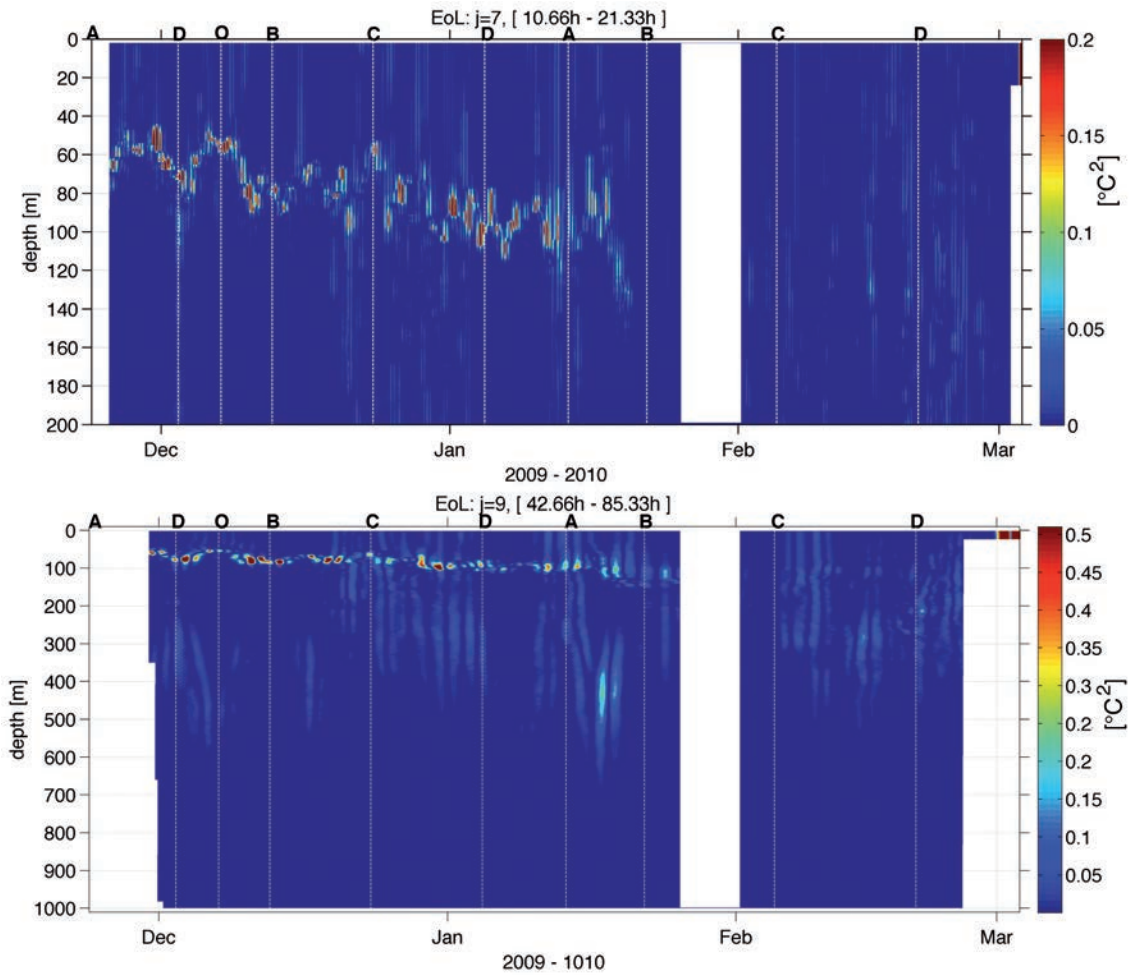
Fig. 16 - Selected timescales from the EoL wavelet analysis. Higher variability in the thermocline is visible in both panels. Lower panel: local maxima appear between 400 and 500 m of depth at timescales of between 42.66 and 85.33 h, i.e., 1.75 and 3.54 days.

500 m of depth, in the transect "AB" through the Cyprus Eddy. Towards the end of the EoL mission, the signature at the thermocline area seems to disappear, indicating a mixing process in the wintertime.

5.3. The buoyancy frequency

The buoyancy frequency is computed for the three missions. This quantity, also called the Brunt-Vaisala frequency, describes the oscillation of a vertically displaced parcel of water in a statically steady medium; hence it is more significant when strong stratification is present, such as during the L10 and T09 missions.

Internal gravity waves may occur in the interface between two different layers, or in a gradually stratified water mass. The frequency of these motions lies between the Coriolis frequency (inertial motion) and the Brunt-Vaisala frequency (buoyancy oscillation). Brunt-Vaisala maps are computed for the three missions (Fig. 17). In L10, the minimum Brunt-
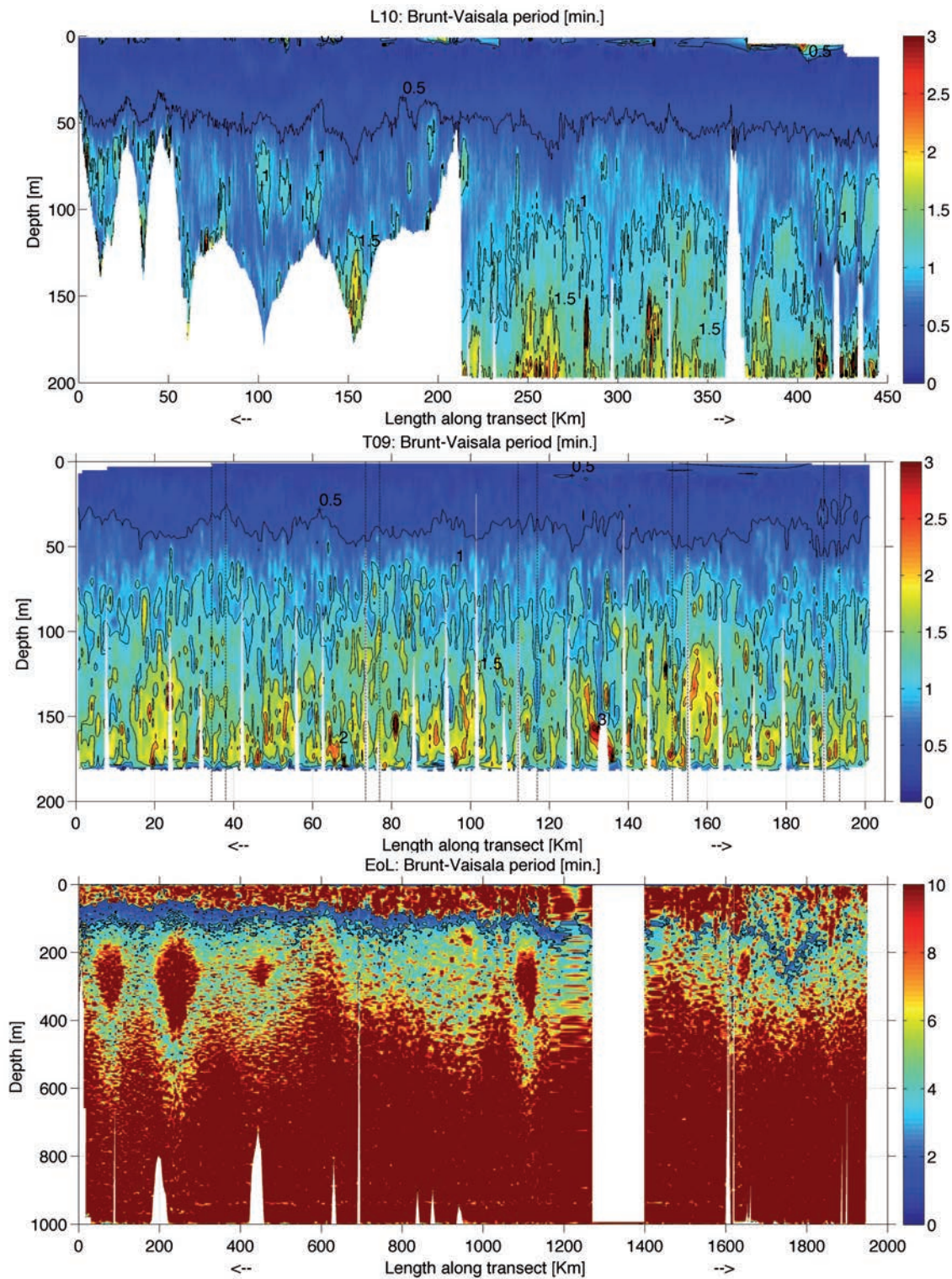
Fig. 17 - Brunt-Vaisala maps from L10 (upper panel), T09 (mid), and EoL (lower panel).

Vaisala period (or maximum frequency) is estimated as 0.5 minutes (or 120 cph), reached at about 30 m of depth. The energy found in this range could be related to internal waves in the thermocline; however, further investigation is required to provide definitive proof. The maximum frequency is reached at the thermocline in T09 and EoL as well. The L10 and T09 missions were performed during strong stratification conditions, so strong internal waves might be expected. However, since the Brunt-Vaisala frequency is beyond the upper boundary of physical significance, internal waves can be observed between the inertial frequency and the upper boundary. Internal waves with higher frequency may exist but cannot be detected. EoL mission was carried out from late autumn 2009 throughout the 2010 winter season, i.e., not the best period to observe stratification because mixing and vertical motions are expected. The EoL Brunt-Vaisala map presented in Fig. 17 (lower panel), does indeed show a transition after travelling 1500 km, corresponding to the last two transects, "CD" and "DA", in February 2010, when the minimum period layer is affected by winter dynamics.

6. Conclusions

Gliders produce an impressive quantity of information, an improvement over other technologies. However, it is necessary to consider a number of factors in order to process the data correctly and obtain significant conclusions. Position, velocity, and the time for the instrument to complete a cycle of a down-cast/up-cast profile are important to consider, as well as the time to complete one transect and the trajectory given in the mission.

The Fourier and wavelet transforms provide useful information when used complementarily, because one overcomes the limitations of the other.

The Fourier spectra from the three missions show a broadening of the energy distribution (Fig. 3) along the frequency axis, at certain depths identified as the thermocline. Comparison among a number of spectra at these depths with several from 'outside the thermocline' (Figs. 4, 8, and 10) illustrates this effect, owing to the Fourier limitations, as reported in mathematical literature (Mallat, 1999). Any transient feature such as discontinuities, decaying waves, *et similia*, still has to be expressed as a sum of permanent sinusoids; this causes the coefficients of the Fourier spectra to decay slowly when such nonstationary features are present. The Fourier formulation tends to "smooth" spectral information and distribute it over the entire range of frequencies. Previous experimental work has actually shown that the rate of decay is connected to the presence of high frequency variability in the spectra (Rudnick and Cole, 2011). An example of this is the irregularity detected in L10 on July 12, 2010: a energy peak at about 8 m of depth (Fig. 7) is connected to a slower decay of the corresponding spectra (Fig. 4), as compared to spectra from deeper layers. Likewise, the sudden deepening of the isotherms in T09 on May 27, 2009 (Fig. 2) is linked to a slower decay of the respective spectra (Fig. 8). Fourier spectra of vertical excursions of temperature have been previously used to study vertical water motions in moorings located in deep trenches in the Ionian Sea (van Haren and Gostiaux, 2011). The amplitude of such excursions can reach up to 250 m in the weakly stratified environment of the trenches. That order of magnitude, measured via a dense array of high-precision temperature sensors, is not possible in the very stratified waters found in the missions presented here. However, it is still possible to investigate vertical motions by using temperature variations

along the water column as long as the currents are not dominated by nonlinearities (van Haren, 2008). Glider records are not limited to a specific point and offer information on wider areas, by comparison.

The wavelet transform can improve the preceding assessment, since it is based on short-lived oscillations, so that its coefficients are relatively high in the vicinity of the transient feature while quickly decaying outside. This property allows the localization of such features in the series and consequent relation of them to physical reality. The main drawback is a loss in frequency resolution as the representation turns to period intervals (timescales), instead of punctual frequencies. The filtering nature of the integral also makes boundary effects appear, further increasing the loss of information in the edges. Despite these limitations, Fourier and wavelet transforms have proved very useful when used together, particularly to evaluate the nature of the features being found, whether they are a natural structure, a by-product of the experimental design (sampling scheme, glider trajectory, etc.), or an instrumental failure. In the Fourier spectra, anomalous features generate a slow decay of energy, whereas using wavelets irregularities are localized in time and space. Similar results can be observed in T09 with sudden changes in the isotherms; the wavelet coefficients keep track of the changes.

While it is recommended to analyse nonstationary variability, wavelet coefficients alone by no means provide a definitive conclusion on the nature of features. More information has to be integrated in order to know whether said features correspond to a propagating wave, or are rather stationary structures, and to find spatial or temporal coherence that may identify a forcing mechanism (Ursella *et al.*, 2014). The manner of execution of the experiment itself introduces most of the possible nuisances and noise, especially when searching for frequency content in the data. However, we demonstrated that the energy of the spurious oscillations is several orders of magnitude less than the one in the real data. The coefficients from the feature found in L10 at 40 m of depth on July 9 (Fig. 12) have relatively high energy because the glider is temporarily entering a different water mass (Fig. 13), decaying quickly as the glider goes out of it. The result is a transient feature in the data.

In Rudnik *et al.* (2013), the internal waves were studied using spatial averaging spectra of potential density under conditions of coherence along the vertical profile in the south of China Sea. The averaged up and down cast spectra and the physical relationship between temperature and salinity, as tackled by Munk (1981), gave additional information to the analysis, producing frequency spectra covering five decades and the whole water column. The methods presented in this paper have been applied in a different way from the aforementioned work, taking advantage of the stratification that temperature records show during certain periods. The computing of layer-by-layer spectra and the localisation of features by the wavelet transform can be related to specific phenomena occurring in the sea. The Brunt-Vaisala frequency complemented the information and were consistent with a scenario where internal waves may occur. However, in the present work, they do not constitute a definitive proof of their existence, since the maximum buoyancy frequency is beyond the upper limit of significance and the variability between I and UB may correspond to a partial signature of the internal waves.

REFERENCES

Bishop C.M.; 2008: *Sensor dynamics of autonomous underwater glider.* PH.D. Thesis in Science for the Environmental Science Program, Memorial University of Newfoundland, Newfoundland, Canada, 150 pp.

Daubechies I.; 1992: *Ten lectures on wavelets.* Soc. Ind. Appl. Math, Philadelphia, PA, USA, 377 pp.

Eriksen C.C., Osse T.J., Light R.D., Wen T., Lehman T.W., Sabin P.L., Ballard J.W. and Chiodi A.M.; 2001: *Seaglider: a long-range autonomous underwater vehicle for oceanographic research.* J. Oceanic Eng., **26**, 424-436.

Garau B., Ruiz S., Zhang W.G., Pascual A., Heslop E., Kerfoot J. and Tintoré J.; 2011: *Thermal lag correction on slocum CTD glider data.* J. Atmos. Oceanic Tech., **28**, 1065-1071, doi:10.1175/JTECH-D-10-05030.1.

Hayes D.R., Zodiatis G., Konnaris G., Hannides A., Solovyov D. and Testor P.; 2011: *Glider transects in the Levantine Sea: characteristics of the warm core Cyprus Eddy.* In: Proc. OCEANS 2011 IEEE, Santander, Spain, pp. 1-9, doi:10.1109/Oceans-Spain.2011.6003393.

Jenkins G. and Watts D.; 1968: *Spectral analysis and its applications.* Holden-Day, San Francisco, CA, USA, 525 pp.

Mallat S.; 1999: *A wavelet tour of signal processing, 2nd edition.* Academic Press, Cambridge, MA, USA, 637 pp.

Mauri E., Bolzon G., Bubbi A., Brunetti F., Gerin R., Medeot N., Nair R., Salon S. and Poulain P.M.; 2010: *High-resolution glider measurements around the Vercelli Seamount (Tyrrhenian Sea) in May 2009.* In: Extended abstract, 39th CIESM Congress, Venezia, Italy, p. 141, <www.ciesm.org/online/archives/abstracts/pdf/39/PG_0141.pdf>

Mauri E., Gerin R., Mancero I. and Poulain P.M.; 2013: *The Ligurian dispersion experiment 2010 (LIDEX10): satellite, drifter and glider preliminary results.* In: Extended abstract, 40th CIESM Congress, Marseille, France, p. 136, <www.ciesm.org/online/archives/abstracts/pdf/40/Vol40_opt.pdf.>.

Munk W.; 1981: *Internal waves and small-scale processes.* In: Warren B.A. and Wunsch C. (eds), Evolution of Physical Oceanography, MIT Press, Cambridge, MA, USA, pp. 264-291.

Press W.H., Teukolsky S.A., Vetterling W.T. and Flannery B.P.; 1992: *Numerical recipes in C: the art of scientific computing*, *2nd edition.* Cambridge Univ. Press, New York, NY, USA, 1178 pp.

Rudnick D.L. and Cole S.R.; 2011: *On sampling the ocean using underwater gliders.* J. Geophys. Res., **116**, C08010, doi:10.1029/2010JC006849.

Rudnick D.L., Davis R.E., Eriksen C.C., Fratantoni D.M. and Perry M.J.; 2004: *Underwater gliders for ocean research.* Mar. Tech. Soc. J., **38**, 48-59.

Rudnick D.L., Shaun Johnston T.M. and Sherman J.T.; 2013: *High-frequency internal waves near the Luzon Strait observed by underwater gliders.* J. Geophys. Res., **118**, 774-784.

Ursella L., Kovačević V. and Gačić M.; 2014: *Tidal variability of the motion in the Strait of Otranto.* Ocean Sci., **10**, 49-67, doi:10.5194/os-10-49-2014.

van Haren H.; 2008: *A comparison between vertical motions measured by ADCP and inferred from temperature data.* Ocean Sci., **4**, 215-222, doi:10.5194/os-4-215-2008.

van Haren H. and Gostiaux L.; 2011: *Large internal waves advection in very weakly stratified deep Mediterranean waters.* Geophys. Res. Lett., **38**, L22603, doi:10.1029/2011GL049707.

Corresponding author: Isaac Mancero-Mosquera
                            Facultad de Ciencias Naturales y Matemáticas, Escuela Superior Politécnica del Litoral
                            Km. 30.5 Vía Perimetral, Guayaquil, Ecuador
                            Phone: +593 4 2269269; e-mail: mancero@espol.edu.ec